An Assessment of the Laminar Kinetic Energy Concept for the Prediction of High-Lift, Low-Reynolds Number Cascade Flows

Article *in* Proceedings of the Institution of Mechanical Engineers Part A Journal of Power and Energy · November 2011

DOI: 10.1177/0957650911412444

CITATIONS
27

READS
431

4 authors:

Roberto Pacciani
University of Florence
90 PUBLICATIONS **1,107** CITATIONS
SEE PROFILE

Michele Marconcini
University of Florence
149 PUBLICATIONS **1,397** CITATIONS
SEE PROFILE

Andrea Arnone
University of Florence
196 PUBLICATIONS **2,703** CITATIONS
SEE PROFILE

Francesco Bertini
AvioAero
90 PUBLICATIONS **957** CITATIONS
SEE PROFILE

An assessment of the laminar kinetic energy concept for the prediction of high-lift, low-Reynolds number cascade flows

R Pacciani[1]*, **M Marconcini**[1], **A Arnone**[1], and **F Bertini**[2]
[1]Department of Energy Engineering, University of Florence, Firenze, Italy
[2]Avio S.p.A., Rivalta di Torino, Italy

The manuscript was received on 28 April 2011 and was accepted after revision for publication on 13 May 2011.

DOI: 10.1177/0957650911412444

Abstract: The laminar kinetic energy (LKE) concept has been applied to the prediction of low-Reynolds number flows, characterized by separation-induced transition, in *high-lift* airfoil cascades for aeronautical low-pressure turbine applications. The LKE transport equation has been coupled with the low-Reynolds number formulation of the Wilcox's $k-\omega$ turbulence model. The proposed methodology has been assessed against two high-lift cascade configurations, characterized by different loading distributions and suction-side diffusion rates, and tested over a wide range of Reynolds numbers. The aft-loaded T106C cascade is studied in both high- and low-speed conditions for several expansion ratios and inlet freestream turbulence values. The front-loaded T108 cascade is analysed in high-speed, low-freestream turbulence conditions. Numerical predictions with steady inflow conditions are compared to measurements carried out by the von Kármán Institute and the University of Cambridge. Results obtained with the proposed model show its ability to predict the evolution of the separated flow region, including bubble-bursting phenomenon and the formation of open separations, in high-lift, low-Reynolds number cascade flows.

Keywords: laminar kinetic energy, high lift, separated-flow transition, low Reynold's number, cascade flows

1 INTRODUCTION

The requirements of lighter jet engine designs, with fewer components but still with a high efficiency level, leads, for the low-pressure (LP) turbine, to a reduction of the number of blades per stage and therefore increased blade loading. LP turbine blades work with relatively low Reynolds numbers and such flow conditions may be particularly critical for the suction-side boundary layer, which is responsible for the greatest contribution to the profile loss (up to 85%). On isolated blade rows, low-Reynolds number operations are likely to produce boundary-layer separation in regions of adverse pressure gradient, and important loss enhancements are associated with these circumstances. In the multistage engine environment, the unsteady wake-induced transition plays a key role in reducing the separation effects up to a level compatible with acceptably low losses. Many studies demonstrate how high-lift [**1**, **2**] and ultra-high-lift [**3**, **4**] airfoils can be operated with loss control by taking advantage of wake-induced transition in LPT low-Reynolds, number flows. The study of wake-induced transition in LP turbines has thus led to improvements in performance of present-generation turbomachinery [**5**, **6**]. With a reduction of the suction-side separation effects, now recognized as the basic mechanism providing increased blade

*Corresponding author: *Department of Energy Engineering, University of Florence, via di Santa Marta 3, 50139, Firenze, Italy. email: roberto.pacciani@unifi.it*

load at acceptably low loss levels, designers and researchers are now looking for other flow-control devices in order to keep supporting and enhancing the high-lift concept [**7**, **8**]. To assess the benefits arising from the use of such devices and/or of wake-induced transition, it is important to be able to compute separation bubbles in isolated cascades with steady inflow and hence the resulting loss levels.

Separation bubbles are commonly classified as 'short' and 'long' [**9**, **10**]. Short bubbles occur at higher Reynolds numbers, and are expected to have only a local effect on the pressure distribution. The formation of a long bubble arises predominantly at low Reynolds numbers, and this tends to influence the pressure distribution along the entire blade surface. The switching of the bubble structure from the short-to-long configuration usually occurs in high lift airfoils when decreasing the Reynolds number, and it is usually referred to as bursting [**9**, **10**]. Such a phenomenon occurs in quite a sudden manner when the Reynolds number goes below a certain critical value. The possibility of predicting the effects of bursting is crucial to analysing the performance of high-lift LP-turbine airfoils. In fact, the associated strong increase in losses could suggest the implementation of passive/active flow control concepts in order to obtain acceptable efficiency levels in practical applications.

Today, turbulence closure in industrial computational fluid dynamic codes are mainly based on one- or two-equation models. However, several studies like the ones of Menter *et al.* [**11**], Langtry *et al.* [**12**], Kožulović *et al.* [**13**], and Suzen *et al.* [**14**] have shown that they can be inefficient, or barely adequate when dealing with flows affected by separation-induced transition mechanisms. A number of approaches have been proposed to address this problem. The majority of the approaches to modelling separated-flow transition are based on the intermittency concept. Menter *et al.* [**11**] have coupled transport models for the intermittency and the transition-onset Reynolds number to obtain a dynamic description of the transition, which makes use of local variables only. More recent methodologies which are based on the concept of the transport of laminar kinetic energy (LKE), are theoretically more general, i.e. they do not rely on global quantities or correlations. They are able to address the rise of pre-transitional fluctuations in boundary layers and their subsequent breakdown to turbulence. Walters and Leylek [**15**, **16**] and Lardeau *et al.* [**17**] exploited the LKE concept, originally introduced by Mayle and Schultz [**18**], to make a two-equation model sensitive to the onset of natural and bypass transition. Examples of successful applications of the LKE approach to LP turbines have been provided by Lardeau and Leschziner [**19**] and Pacciani *et al.* [**20**, **21**]. This article assesses the application of a new LKE model to the calculation of high-lift cascades tested in LP turbine conditions. The well-known T106 and the T108 cascades are used to assess the ability of the present model to predict transitional low-Reynolds number flows around LP turbine blades. Such high-lift cascades have recently been tested experimentally within the framework of two European research projects (UTAT and TATMo). Low-speed tests were conducted at the University of Cambridge [**22**] while high-speed measurements were provided by the von Kármán Institute [**23**]. The results of the numerical investigations are discussed with reference to a broad range of flow conditions, with different Reynolds numbers, expansion ratios, and freestream turbulence intensities. Particular emphasis will be devoted to the discussion of the capabilities of the present approach to predict the occurrence of both short and long bubbles.

2 COMPUTATIONAL FRAMEWORK

The time-accurate release of the TRAF code [**24**] was used in this study. The unsteady, three-dimensional, Reynolds averaged Navier–Stokes (RANS) equations are written in conservative form in a curvilinear, body-fitted coordinate system and solved for density, absolute momentum components, and total energy. A dual-time stepping method [**25**] is used to perform time accurate calculations.

2.1 Transition and turbulence modelling

The proposed model, denoted as LKE model hereafter, is based on the laminar kinetic energy concept originally introduced by Mayle and Schultz [**18**], which enables to take into account the pre-transitional rise of the fluctuating kinetic energy. The modelled transport equation for the LKE is written as [**17**, **21**]

$$\frac{Dk_\ell}{Dt} = \nu_\ell S^2 - 2\nu\frac{k_\ell}{y^2} + \nu\nabla^2 k_\ell \tag{1}$$

The quantity ν_ℓ is the laminar eddy-viscosity, and is modelled as follows

$$\nu_\ell = C_1 f_1 \sqrt{k_\ell}\delta_\Omega \tag{2}$$

with $C_1 = 0.01$ deduced from calibration, and

$$f_1(Tu) = \max\left\{0.8, 2.0\cdot\tanh\left[\left(\frac{Tu}{4.5}\right)^{\frac{1}{2}}\right]\right\} \tag{3}$$

Once the laminar kinetic energy is created in the separated shear layer, it must be transferred to the

turbulence field to trigger the transition process, as shown by numerical [**26**] and experimental investigations [**27**]. The laminar and turbulent kinetic energy equations can be written in a general form as follows

$$\frac{Dk_\ell}{Dt} = \nu_\ell S^2 - 2\nu\frac{k_\ell}{y^2} + \nu\nabla^2 k_\ell - R \tag{4}$$

$$\frac{Dk}{Dt} = P_k - \beta^* k\omega + \frac{\partial}{\partial x_j}\left[(\nu + \sigma_k \nu_T)\frac{\partial k}{\partial x_j}\right] + R \tag{5}$$

The term R appears in both equations, but with opposite signs, resulting in no net change of the total fluctuating kinetic energy $k_{tot} = k_\ell + k$. Rather there is a transfer of energy from k_ℓ to k. Following Walters and Leylek [**15**], this term is assumed to be proportional to k_ℓ

$$R = C_2 f_2 \omega k_\ell \tag{6}$$

The damping function f_2 is defined as follows

$$f_2 = 1 - e^{-\psi/C_3} \tag{7}$$

$$\psi = \max\left(0;\, R_y - C_4\right) \tag{8}$$

The constants are $C_2 = 0.3$, $C_3 = 8$, and $C_4 = 10$. The quantity ψ can be considered as a transition parameter, because it controls the transfer of energy from the laminar to the turbulent state, which occurs when the Reynolds number R_y reaches the threshold value C_4.

The LKE model is then applied in combination with the classical Wilcox low-Reynolds number $k-\omega$ model [**28**], which is widely used in turbomachinery calculations.

The inlet condition for k_ℓ is as follows: $k_{\ell\infty} = k_\infty = 3/2 \cdot Tu_\infty^2 \cdot u_\infty^2$ (see reference [**18**] for more details).

3 THE T106C TURBINE CASCADE

The T106 blade section [**29**] is a widely used geometry for both experimental and numerical studies on high-lift LP profiles. Detailed experimental data are available for a range of incidence, cascade solidity and Reynolds number. The T106C cascade is obtained by imposing a pitch-to-chord ratio of $s/c = 0.95$. A 593×97 non-periodic O-type mesh, like in Pacciani *et al.* [**20**], has been selected for the analysis. The y^+ values of the mesh nodes closest to the wall were below unity in the turbulent part of the blade boundary layer. Indeed, numerical results were verified to be grid independent. Convergence was assumed when the RMS value of the residuals reached the single precision machine zero. The maximum value of the residuals norm was of the order 1×10^{-6}. Such a convergence level required a number of 1000 multigrid cycles to be reached for all the considered Reynolds numbers. A wide range of flow conditions have been considered. They include low-speed (incompressible) operation, high-speed conditions with different cascade expansion ratios, and several inlet turbulence intensity values. The inlet turbulent length scale was deduced in order to guarantee the correct turbulence decay upstream of the cascade, and a non-dimensional value of $\ell_{T\infty}/c_x = 2.5 \times 10^{-3}$ was prescribed.

The discussion of the numerical results will be split in two subsections. The first will be devoted to the analysis of the cascade in low-speed conditions, as tested experimentally at the University of Cambridge [**22**], while in the second the predictions in high-speed conditions will be compared to the measurements carried out at the VKI [**23**]. For the low-speed data, the maximum uncertainty was reported to be around 1 per cent for the pressure coefficient, and between 0.5 per cent and 2 per cent for the total pressure loss coefficient. For the high-speed data, relative uncertainties on the kinetic energy losses were reported ranging between 10-20 per cent. The absolute flow angle uncertainty varied between 0.2 and 0.3°. Relative uncertainties on isentropic Mach number ranged between 0.4 per cent-1.2 per cent.

3.1 Low-speed computations

Several Reynolds number values, ranging from 0.5×10^5 to 2.1×10^5 were investigated, together with two different freestream turbulence intensities corresponding to $Tu_\infty = 0.4$ per cent and $Tu_\infty = 4.0$ per cent. The computed pressure coefficient distributions on the blade surface, for six different values of the Reynolds number, are compared to experiments in Fig. 1(a) to (f). The agreement is very good for all the cases, and only minor discrepancies are recorded for the lowest Reynolds number values ($Re_{2,is} = 0.5 \times 10^5$). In particular, the effects of the separation are well reproduced by the calculations.

For the lowest level of the freestream turbulence intensity ($Tu_\infty = 0.4$ per cent), and in the range between $Re_{2,is} = 2.1 \times 10^5$ and $Re_{2,is} = 1.2 \times 10^5$, gradual modifications occur in the blade-loading distributions when the Reynolds number is decreased. This suggests the presence of a short bubble, undergoing a correspondingly gradual increase in size. On the contrary, the remarkable changes in the blade loading distribution for $Re_{2,is} = 0.9 \times 10^5$, with respect to the cases at higher Reynolds numbers, indicate the formation of a long bubble. A further lowering of the Reynolds number results in an open separation, as no flow reattachment is detected for $Re_{2,is} \leqslant 0.7 \times 10^5$. The appearance of bubble bursting is generally associated with Reynolds number values which are below a certain critical value. Such a value

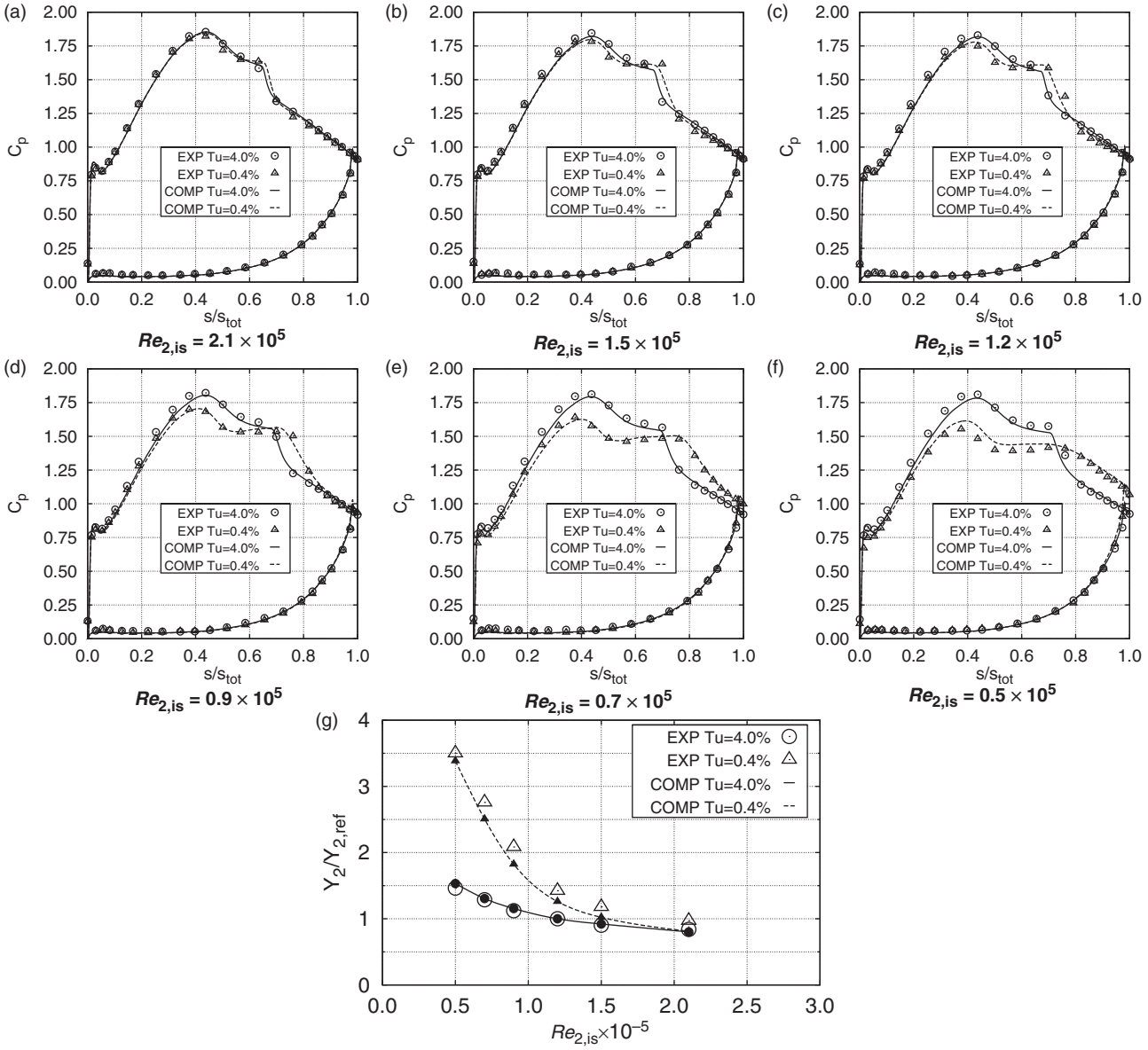

Fig. 1 T106C cascade: Pressure coefficient distributions (a)–(f) and normalized mixed-out total-pressure loss coefficient as a function of $Re_{2,is}$ (g)

is then expected to occur between $Re_{2,is} = 1.2 \times 10^5$ and $Re_{2,is} = 0.9 \times 10^5$ at the lowest inlet turbulence intensity. The bursting effect appears to be correctly detected by the proposed model.

The behaviour of the suction-side boundary layer and separated flow region is noticeably different when the inlet turbulence level is increased from $Tu_\infty = 0.4$ per cent to $Tu_\infty = 4.0$ per cent. Generally speaking, a freestream turbulence increase results in a reduction of the extension of the separated flow region [**23**]. For the cascade under investigations, both experimental and numerical results indicate that the most pronounced impact takes place for the lower Reynolds number values. For $Re_{2,is}$ values between 0.5×10^5 and 0.9×10^5, the increase in the freestream turbulence level results in a very strong contraction of the separated flow region. The open separation that exists for $Tu_\infty = 0.4$ per cent becomes a short bubble for $Tu_\infty = 4.0$ per cent. Such a circumstance can be deduced from the pressure coefficient distributions of Fig. 1 that shows the evidence of flow reattachment, for $Tu_\infty = 4.0$ per cent, even for the lowest Reynolds number value ($Re_{2,is} = 0.5 \times 10^5$, Fig. 1(f)).

At higher Reynolds numbers ($Re_{2,is} \geqslant 1.2 \times 10^5$), an increase in the freestream turbulence intensity results in a much weaker effect on the separated flow region, with small reductions of its extension

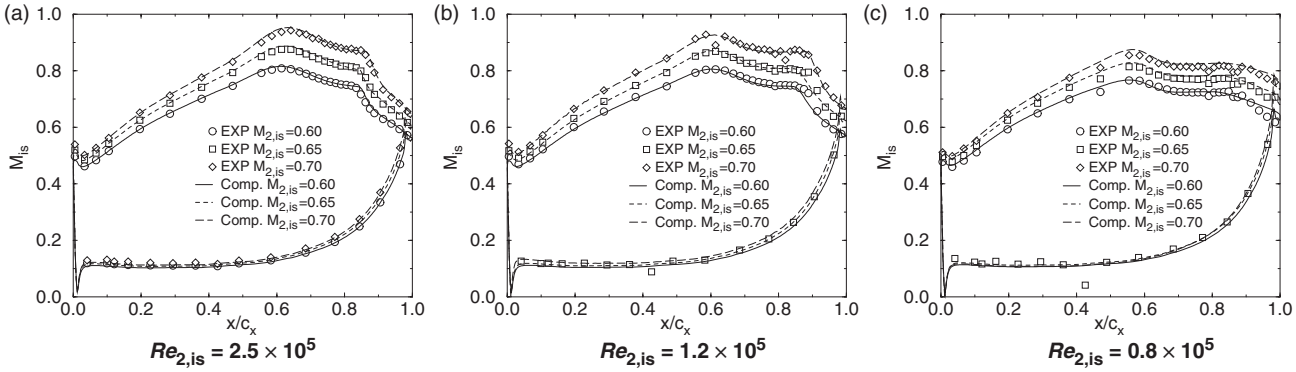

Fig. 2 T106C cascade: isentropic Mach-number distributions

and no appreciable change in structure. The small difference that can be detected in terms of pressure coefficient distributions in the separated flow region between the cases at $Tu_\infty = 0.4$ per cent and $Tu_\infty = 4.0$ per cent for $Re_{2,is} = 1.2 \times 10^5$ becomes practically negligible for $Re_{2,is} = 2.1 \times 10^5$ (Fig. 1(a) to (c)). It is worth noticing how the experimental evidence of the freestream turbulence impact is very well reproduced by the proposed methodology.

As far as bubble bursting is concerned, the increase in the freestream turbulence level was also found to be responsible for a decrease of the critical Reynolds number. Such a circumstance can be appreciated in Fig. 1(g), where the cascade lapse rates are reported for the investigated Tu_∞ values. The agreement between computed and measured values is again remarkable. For the case of $Tu_\infty = 0.4$ per cent the cascade losses undergo an abrupt increase in their rates of change in the critical range of the Reynolds number, and this is associated with the occurrence of bubble bursting.

By increasing the Tu_∞ value to 4.0 per cent, the total-pressure loss coefficient is reduced in the whole range of analysed Reynolds numbers. Such a reduction becomes larger and larger as the Reynolds number is decreased and it becomes extremely significant for $Re_{2,is} < 1.5 \times 10^5$. A much more favourable lapse rate at high freestream turbulence intensity is expected to be associated with the contraction of the separation bubble, and with the fact that bubble bursting occurs for lower values of the Reynolds number with respect to the considered range.

3.2 High-speed computations

Three different expansion ratios, leading to exit isentropic Mach number values of $M_{2,is} = 0.6$, $M_{2,is} = 0.65$, and $M_{2,is} = 0.7$ were considered. The corresponding isentropic Mach number distributions on the blade surface, for four different values of the Reynolds number, are compared to experiments in Fig. 2. Measured data have been obtained with a freestream turbulence level of $Tu_\infty = 0.8$ per cent. The agreement is very good for all the cases. In particular, the effects of the separation on the isentropic Mach-number distribution are correctly reproduced by the calculations, and small discrepancies arise only at the lower Reynolds numbers, in the pressure-recovery region of the bubble. Here, the calculations tend to predict a slightly smoother pressure gradient with respect to the experiments (Fig. 2(c)). For a given Reynolds number, the increase of the exit Mach number results in an enhancement of the separation-related effects. This would suggest that the bubble is growing with the exit Mach number itself, and it is consistent with the increase in the suction-side diffusion rate due to the increase of the expansion ratio. In the range between $Re_{2,is} = 2.5 \times 10^5$ and $Re_{2,is} = 1.2 \times 10^5$, the separated flow region appears to have the structure of a short bubble for all the investigated expansion ratios. The situation is quite different at $Re_{2,is} = 1.2 \times 10^5$, as it can be deduced from Fig. 3, which reports streamlines superposed on turbulent kinetic energy contours in the separated flow region, for the three considered expansion ratios. The cases corresponding to $M_{2,is} = 0.6$, $M_{2,is} = 0.65$ are still characterized by typical short bubble configurations. On the contrary, the case with the highest expansion ratio shows the occurrence of bubble bursting. The relevant increase in length of the separated flow region, produced by the displacement of the reattachment location towards the trailing edge, moves the flow configuration into the domain of long bubbles. Transition occurs in harmony with the location of maximum bubble thickness, and this increases with the exit Mach number. As a consequence, the maximum turbulent energy production in the breakdown region occurs at increasing distance from the wall and, at the highest expansion ratio, the resulting turbulence field is not effective for producing a rapid reattachment.

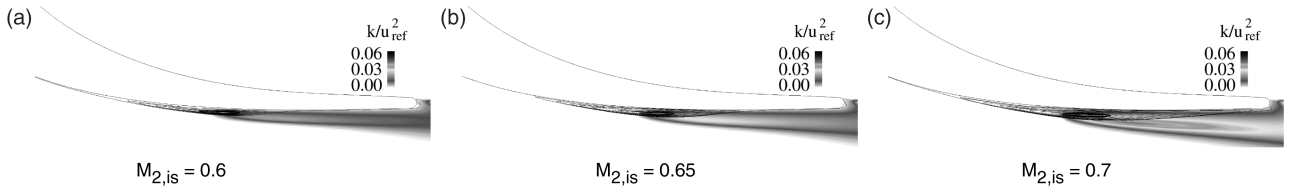

Fig. 3 T106C cascade: separation bubble configurations at different exit isentropic Mach numbers for $Re_{2,is} = 1.2 \times 10^5$

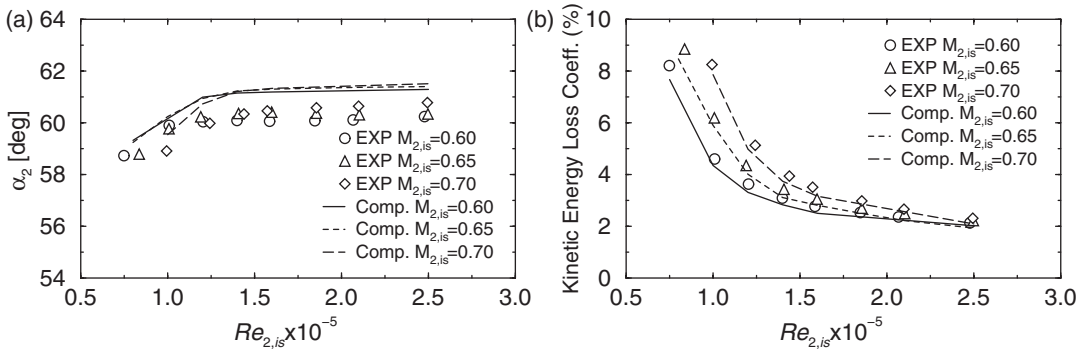

Fig. 4 T106C cascade: (a) exit flow angle and (b) kinetic energy loss coefficient (%) as a function of $Re_{2,is}$

The substantial modification in the blade-load distribution, observable for $Re_{2,is} \leqslant 1.0 \times 10^5$, relative to the cases at the higher Reynolds numbers, suggests that the separated flow region has become a long bubble for all the considered expansion ratios. Indeed, the flow is not even reattached in the case at the lowest Reynolds number ($Re_{2,is} = 0.8 \times 10^5$), indicating the presence of an open separation rather than a long bubble.

The critical Reynolds number for bubble bursting is then predicted to occur between $Re_{2,is} = 1.2 \times 10^5$ and $Re_{2,is} = 1.0 \times 10^5$ for the T106C cascade in high-speed conditions, and it is found to increase when increasing the cascade expansion ratio. The correct prediction of the phenomena associated with bursting can also be assessed from the lapse rates of Fig. 4. Cascade lapse rates, in terms of the computed exit flow angle and kinetic energy loss coefficient as a function of $Re_{2,is}$ are compared to the corresponding measured data in Fig. 4. The difference between the computed and experimental flow angle is below 1.0°, while losses are only mildly underestimated at low Reynolds numbers. The exit flow angle remains almost constant for Reynolds number values which are above the critical one. When $Re_{2,is}$ is below this value, the exit flow angle rapidly decreases. Both computed and experimental loss coefficients undergo an abrupt increase in their rates of change in the critical range of the Reynolds number. Consistent with the previous observations, such an increase occurs at higher Reynolds numbers for higher expansion ratios.

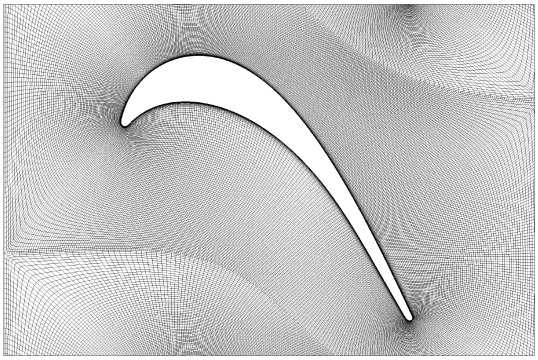

Fig. 5 T108–O-type grid 593 × 97

4 THE T108 TURBINE CASCADE

The T108 cascade is a high-lift configuration, which was tested experimentally at the von Kármán Institute as part of the TATMo research project. The airfoil geometry and the 593 × 97, non-periodic O-Type grid used for the calculations are shown in Fig. 5. The T108 airfoil is front loaded and, with respect to T106C cascade, it shows a much more gradual diffusion from the suction velocity peak to the blade trailing edge. At all the Reynolds numbers, the separation bubbles occurring on the blade

suction side were then expected to be smaller than in the previous case. Experiments were conducted for an exit isentropic Mach number value of $M_{2,is} = 0.6$, and the tested Reynolds number values range from $Re_{2,is} = 0.7 \times 10^5$ to $Re_{2,is} = 2.0 \times 10^5$. The main flow conditions analysed in the calculations are summarized in Table 1. The experimental uncertainties were the same as for the T106C high-speed cases.

Figure 6 compares calculated and measured isentropic Mach number distributions along the blade suction side for three different values of the Reynolds number. They suggest that the suction-side boundary layer appears to be mildly separated at the highest Reynolds number, and that the separated flow region has still the structure of a very small bubble even at the lowest Reynolds number. The separation impact on the suction side isentropic Mach number distribution is seen to increase as the Reynolds number decreases, but it appears to have only a local effect, without overall modifications of the distribution itself. This would suggest that the occurrence of bubble bursting is delayed to even lower Reynolds numbers for this blade. The agreement between computations and experiments is very good. Computed lapse rates are compared to experimental ones in Fig. 7. Despite some scattering in the measured exit flow angles, which is not detected in the calculations (Fig. 7(b)), on the average the agreement can be regarded as satisfactory. In particular, both experimental and calculated values show a very gradual decrease when decreasing the Reynolds number in the considered range. Such behaviour is quite different from that of the T106C cascade and it is consistent with the gradual increase in the separation bubble, without bursting phenomena, found for the present cascade. Similar considerations hold for the kinetic energy loss coefficient as a function of the Reynolds number (Fig. 7(a)). The gradual loss increase for decreasing Reynolds number shown by the experimental results is very well reproduced by the computations and no abrupt loss raise due to the appearance of a long bubble can here be appreciated. It can also be noticed how the

Table 1 Main flow parameters for the T108 cascade

α_1	34.7°
s/c	1.05
$M_{2,is}$	0.60
$\ell_{T\infty}/c_x$	2.5×10^{-3}
Tu_∞	1.00%

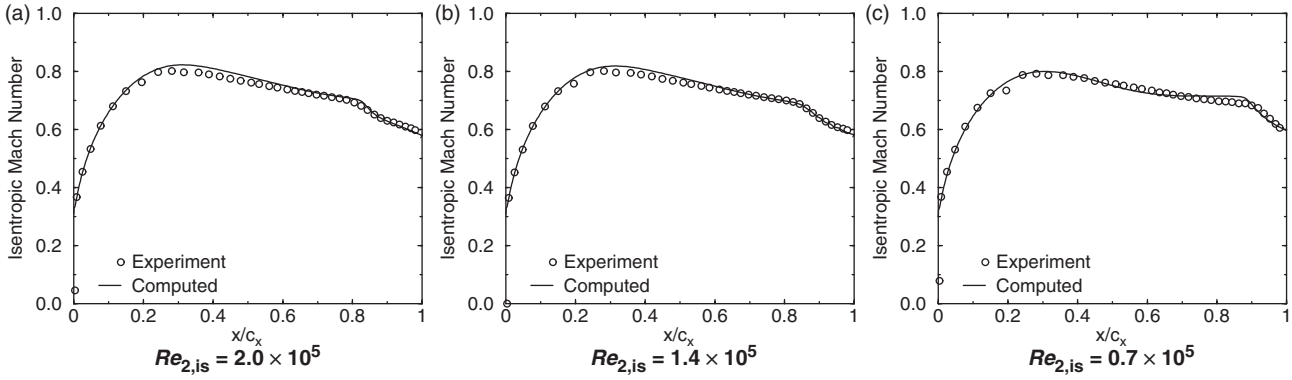

Fig. 6 T108 cascade: isentropic Mach-number distribution

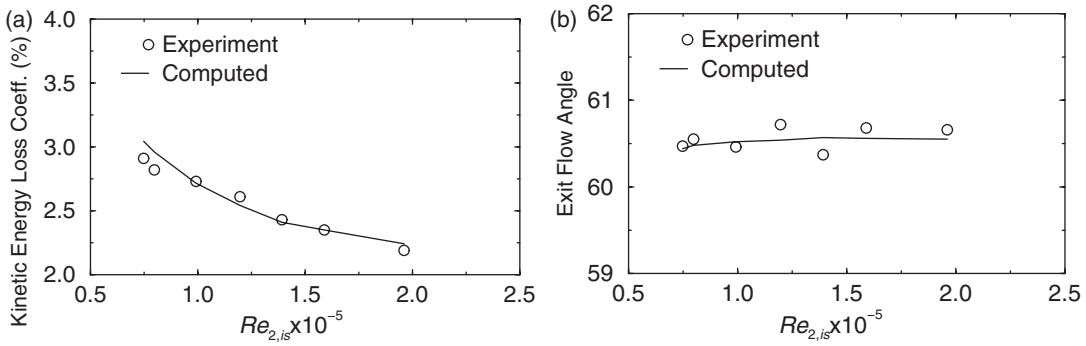

Fig. 7 T108 cascade: kinetic energy loss (%) and exit flow angle as a function of $Re_{2,is}$

loss level is clearly below that of the T106C cascade, especially at low Reynolds number. As reported by other authors [**30**], this is expected to be the result of the different loading distributions of the two high-lift blades. In particular, for the same value of the cascade solidity, a front-loaded design produces a smoother adverse pressure gradient in the diffusing region of the blade suction side, resulting not only in smaller separation bubbles but also displacing the occurrence of bursting below the Reynolds number range of interest in practical applications.

CONCLUSIONS

A new model, based on the laminar kinetic energy concept originally introduced by Mayle and Schultz [**18**], is coupled with a linear eddy-viscosity model to predict separated-flow transition in high-lift cascades operating in conditions representative of those in LP turbines. The novel $k_\ell - k - \omega$ model displays very good performance when applied to the T106C and T108 cascades. The assessment covered a range of Reynolds numbers, expansion ratios, and free-stream turbulence levels, within which short as well as long separation bubbles are produced on the blade suction side. The effect of bubble bursting, in the cases it occurs, is correctly predicted, together with its effects on blade loading distributions, and lapse rates. The study may be claimed to have demonstrated that the proposed model offers an economical and accurate mean of providing affordable engineering predictions of transitional flows in LP turbines, even if a somewhat weaker performance is shown in the very low Reynolds number regime. This is the range of conditions where unsteady flow structure develops on spatial scales that undergo a questionable modelling in the framework of RANS approaches using simple linear eddy-viscosity closures. Fundamental investigations, carried out with approaches that are able to resolve the physical details, and therefore the effects of such structures (i.e. LES or DNS), could be of great help in suggesting further modelling ideas to support and enhance transition-sensitive turbulence closures.

FUNDING

The research study reported in this paper was funded by the European Commission within the research projects TATMo (Contract No. AST5-CT-2006-030939, www.tatmo.eu) and UTAT (contract No. G4RD-CT-2001-00628).

ACKNOWLEDGEMENT

The authors thank their fellow partners in European Union FP6 programme TATMo for permitting the publication of our results in this paper.

REFERENCES

1 **Cobley, K., Coleman, N., Siden, G.,** and **Arndt, N.** Design of new three stage low pressure turbine for the BMW Rolls-Royce BR715 turbofan engine. ASME paper 97–GT–419, Orlando, Florida, 2–5 June 1997.

2 **Curtis, E. M., Hodson, H. P., Banieghbal, M. R., Denton, J. D., Howell, R. J.,** and **Harvey, N. W.** Development of blade profiles for low pressure turbine applications. *ASME J. Turbomach.*, 1997, **119**(3), 531–538.

3 **Haselbach, F., Schiffer, H. P., Horsman, M., Dressen, S., Harvey, N. W.,** and **Read, S.** The application of ultra high lift blading in the BR715 LP turbine. *ASME J. Turbomach.*, 2002, **124**(1), 45–51.

4 **Howell, R. J., Hodson, H. P., Schulte, V., Stieger, R. D., Schiffer, H. P., Haselbach, F.,** and **Harvey, N. W.** Boundary layer development in the BR710 and BR715 LP turbines – the implementation of high–lift and ultra-high-lift concepts. *ASME J. Turbomach.*, 2002, **124**(3), 385–392.

5 **Schulte, V.** and **Hodson, H. P.** Unsteady wake–induced boundary layer transition in high lift LP turbines. *ASME J. Turbomach.*, 1998, **120**(1), 28–35.

6 **Stieger, R. D.** and **Hodson, H. P.** The transition mechanism of highly loaded low-pressure turbine blades. *ASME J. Turbomach.*, 2004, **126**(4), 536–543.

7 **Zhang, F. H., Vera, M., Hodson, H. P.,** and **Harvey, N.** Separation and transition control on an aft-loaded ultra-high-lift LP turbine blade at low reynolds numbers: low-speed investigation. *ASME J. Turbomach.*, 2006, **128**(3), 517–527.

8 **Rumsey, C. L., Gatski, T. B., Sellers III, W. L., Vatsa, V. N.,** and **Viken, S. A.** Summary of the 2004 computational fluid dynamics validation workshop on synthetic jets. *AIAA J.*, 2006, **44**(2), 194–207.

9 **Gaster, M.** The structure and behaviour of laminar separation bubbles. Aeronautical Research Council R&M 3595, 1969.

10 **Lou, W.** and **Hourmouziadis, J.** Separation bubbles under steady and periodic-unsteady main flow conditions. *ASME J. Turbomach.*, 2000, **122**(4), 634–643.

11 **Menter, F. R., Langtry, R. B., Likki, S. R., Suzen, Y. B., Huang, P. G.,** and **Völker, S.** A correlation-based transition model using local variables – Part I: Model Formulation. *ASME J. Turbomach.*, 2006, **128**(3), 413–422.

12 **Langtry, R. B., Menter, F. R., Likki, S. R., Suzen, Y. B., Huang, P. G.,** and **Völker, S.** A correlation-based transition model using local variables – Part II: test cases and industrial applications. *ASME J. Turbomach.*, 2006, **128**(3), 423–434.

13 **Kožulović, D., Röber, T.,** and **Nürnberger, D.** Application of a multimode transition model to turbomachinery flows. In Proceedings of the 7th European Turbomachinery Conference, Athens, Greece, 5–9 March 2007.

14 **Suzen, Y. B., Huang, P. G., Ashpis, D. E., Volino, R. J., Corke, T. C., Thomas, F. O., Huang, J., Lake, J. P.,** and **King, P. I.** A computational fluid dynamics study of transitional flows in low-pressure turbines under a wide range of operating conditions. *ASME J. Turbomach.*, 2007, **129**(3), 527–541.

15 **Walters, D. K.** and **Leylek, J. H.** A new model for boundary layer transition using a single-point RANS approach. *ASME J. Turbomach.*, 2004, **126**(1), 193–202.

16 **Walters, D. K.** and **Leylek, J. H.** Computational fluid dynamics study of wake-induced transition on a compressor-like flat plate. *ASME J. Turbomach.*, 2005, **127**(1), 52–63.

17 **Lardeau, S., Leschziner, M. A.,** and **Li, N.** Modelling bypass transition with low-Reynolds-number nonlinear eddy-viscosity closure. *Flow Turbul. Combust.*, 2004, **73**, 49–76.

18 **Mayle, R. E.** and **Schultz, A.** The path to predicting bypass transition. *ASME J. Turbomach.*, 1997, **119**(3), 405–411.

19 **Lardeau, S.** and **Leschziner, M. A.** Modelling of wake-induced transition in low-pressure turbine cascades. *AIAA J.*, 2006, **44**(8), 1854–1865.

20 **Pacciani, R., Marconcini, M., Arnone, A.,** and **Bertini, F.** A CFD study of low Reynolds number flow in high lift cascades. ASME paper GT2010-23300, Glasgow, UK, 14–18 June 2010, pp. 1525–1534.

21 **Pacciani, R., Marconcini, M., Fadai-Ghotbi, A., Lardeau, S.,** and **Leschziner, M. A.** Calculation of high-lift cascades in low pressure turbine conditions using a three-equation model. *ASME J. Turbomach.*, 2011, **133**(031016).

22 **Himmel, C. G., Thomas, R. L.,** and **Hodson, H. P.** Effective passive flow control for ultra-high lift low pressure turbines. In Proceedings of the 8th European Turbomachinery Conference, Graz, Austria, 23–27 March 2009.

23 **Michálek, J., Monaldi, M.,** and **Arts, T.** Aerodynamic performance of a very high lift low pressure turbine airfoil (T106C) at low Reynolds and high Mach number with effect of free stream turbulence intensity. ASME paper GT2010-22884, Glasgow, UK, 14–18 June 2010.

24 **Arnone, A., Liou, M. S.,** and **Povinelli, L. A.** Navier–Stokes solution of transonic cascade flow using non–periodic c–type grids. *J. Prop. Power*, 1992, **8**(2), 410–417.

25 **Arnone, A.** and **Pacciani, R.** Rotor-stator interaction analysis using the Navier–Stokes equations and a multigrid method. *ASME J. Turbomach.*, 1996, **118**(4), 679–689.

26 **Wissink, J. G.** and **Rodi, W.** Direct numerical simulations of transitional flow in turbomachinery. *ASME J. Turbomach.*, 2006, **128**(4), 668–678.

27 **Hatman, A.** and **Wang, T.** A Prediction model for separated-flow transition. *ASME J. Turbomach.*, 1999, **121**(3), 594–602.

28 **Wilcox, D. C.** *Turbulence modeling for CFD*, 2nd edition, 1998 (DCW Ind. Inc, La Cañada, California, USA).

29 **Hoheisel, H.** Test case E/CA-6 subsonic turbine cascade T106 test cases for computation of internal flows in aero engine components. AGARD-AR-275, 1990.

30 **Coull, J. D., Thomas, R. L.,** and **Hodson, H. P.** Velocity distributions for low pressure turbines. *ASME J. Turbomach.*, 2010, **132**(041006).

APPENDIX

Notation

c	blade chord [m]
C_p	pressure coefficient
k	turbulent kinetic energy [m^2/s^2]
ℓ	length scale [m]
M	Mach number
P	production term [m^2/s^3]
Re_{is}	isentropic Reynolds number, cu_{is}/ν_{is}
R_y	wall-distance turbulent Reynolds number, $\sqrt{k}y/\nu$
s	blade pitch, curvilinear abscissa [m]
S	mean shear rate, $S = \sqrt{2S_{ij}S_{ij}}$ [s^{-1}]
Tu	turbulence level, $100\sqrt{(2/3)k/u^2}$ [%]
u	velocity magnitude [m/s]
x, y, z	Cartesian coordinates [m]
Y	total pressure loss coefficient
α	flow angle [°]
δ_Ω	vorticity thickness, $\frac{u_\infty}{2}\left(\frac{\partial u}{\partial y}\right)^{-1}_{\max_y}$ [m]
ν	kinematic viscosity [m^2/s]
Ω	vorticity magnitude [s^{-1}]
ω	specific turbulence dissipation rate [s^{-1}]

Subscripts

1	inflow
2	outflow
ℓ	laminar
∞	freestream
is	isentropic
ref	reference value
T	turbulent
x	axial direction